# Ghost Imaging of Space Objects

Dmitry V. Strekalov, Baris I. Erkmen and Nan Yu

*Jet Propulsion Laboratory, California Institute of Technology,*
*4800 Oak Grove Drive, Pasadena, California 91109-8099 USA*

*NIAC Phase I Final report*

*September 2012*

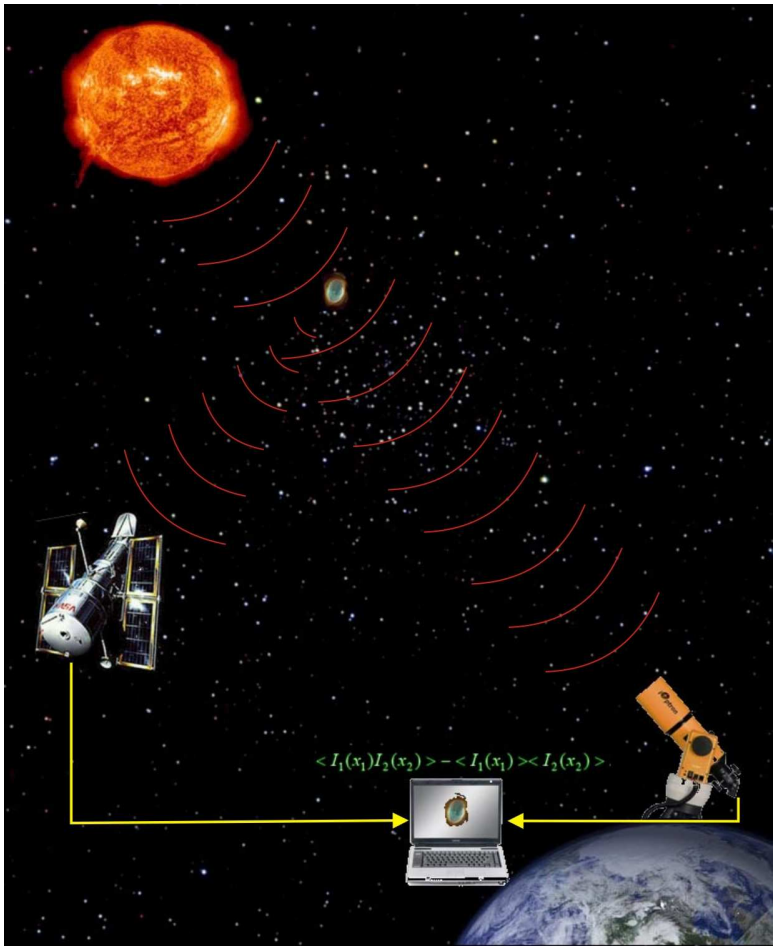


Jet Propulsion Laboratory
California Institute of Technology

CALIFORNIA INSTITUTE OF TECHNOLOGY
1891

## I. ORIGINS AN MOTIVATION OF THIS RESEARCH

Development of innovative aerospace technologies is critical for our nation to meet its goals to explore and understand the Earth, our solar system, and the universe. The spectacular success of many recent NASA missions hinges on the extensive technological innovations that NASA has been supporting for the past decades. To sustain this successful tradition it is very important to identify and stimulate the scientific research that may turn into a viable technology in the decades yet to come. Investment in innovative low-TRL research stimulates the growth of the scientific knowledge and enhances the technical capabilities in a way that answers the new questions and responds to new requirements. Such an investment also stimulates innovation and helps finding novel creative solutions to problems constrained by schedule and budget. Moreover, the impact of this kind of investment goes beyond the specific area. A long-term program of development of advanced space concepts and technology is likely to have multiple positive outcomes. While the most direct of such outcomes are a more exciting science and exploration future and a more robust national capability for aerospace activities, one can also expect this program to enable new industries and contribute to the national economic growth. It will also create innovations that can be applied broadly in a more robust technology-based economy, will serve as an international symbol of our country's scientific achievements and technological growth. The NASA OCT's NIAC program which has sponsored this research effort is an example of such a long-term technological investment. This program has a history of seeding the research efforts that later turned into a great success. One of the most recent and spectacular examples of such an early innovation sponsorship is the Kepler planetary detection research mission [1, 2]. We use the achievements of this mission as benchmarks for our research.

Like the Kepler mission, our research lies in the area of observation astronomy. We aim to improve the technical methods and approaches available in this area and directed to investigation of such important space objects as exoplanets, gravitational lenses, gas and dust clouds, and others. Direct intensity measurement, by an eye or by a detector, has always been the foundation of observation astronomy. Sometimes this technique is successfully complimented by other types of measurements, for example those relying on intensity correlations. The first and perhaps the most famous example of intensity interferometry applied in astronomy is the measurement of angular size of a star by R. Hanbury Brown and R.Q. Twiss in 1957 [3]. Fifty years after this pioneering work, a space-deployable version of this approach has been suggested [4].

Intensity correlation measurements proved to be also important in an extremely distant from astronomy area of science: in quantum optics. In particular, photon coincidence measurements have allowed for the study of nonclassical optical fields whose photons are emitted as tightly correlated pairs, e.g. in a process of parametric down conversion. Parametrically produced photons are not only tightly correlated in time, but also in space, even to the extent beyond possible in classical physics. (This phenomenon is one of the manifestations of the *quantum entanglement*.) This spatial correlation between parametric photons can predict the detectable "location" of one photon based on the observation of the other with a better resolution than a direct intensity measurement. It also enables a remarkable technique of optical imaging, called the "ghost imaging". The quantum world is usually associated with small size and low energy, and is believed to be governed by laws often defying the common sense. Quantum systems make wonderful objects for study, but rarely become tools for the research in other areas of science and engineering. Any such event in the history has had truly revolutionary value. A few relevant examples are the laser, transistor, and superconductivity. It is therefore not surprising that the quantum optical phenomena raised great interest as potential instruments for science and technology. The possibility to surpass the classical limit of optical resolution has been suggested for use in microscopic imaging [5] and lithography [6, 7]. The unique features of ghost imaging were proposed for spectroscopy [8, 9] and for the military surveillance [10] applications. In this research we take a further step and consider a possibility for application of ghost imaging (or speaking more generally, optical correlation imaging) to astronomy. We expect this approach to enhance the conventional observation astronomy capabilities as well as to bring about the capabilities that are conceptually new.

## II. WHAT IS THE GHOST IMAGING AND HOW IT FITS WITH ASTRONOMY OBSERVATIONS

The term "ghost imaging" was coined in 1995 when an optical correlation measurement using biphoton light from parametric down conversion crystal was used to reconstruct an image [11] or diffraction pattern [12] of a mask placed in the *signal* channel by scanning a detector in an empty *idler* channel. This image is obtained by a gated photon counting, with the gating obtained by photon detections in the signal channel which lacks any spatial resolution, as illustrated in Fig. 1.

Besides its significance for the field of quantum optics, the ghost imaging technique has a few appealing practical advantages. Since no spatial resolution in the object channel is required, a very primitive single-pixel optical sensor could be placed in this channel, with the more advanced optics responsible for the image quality placed in the

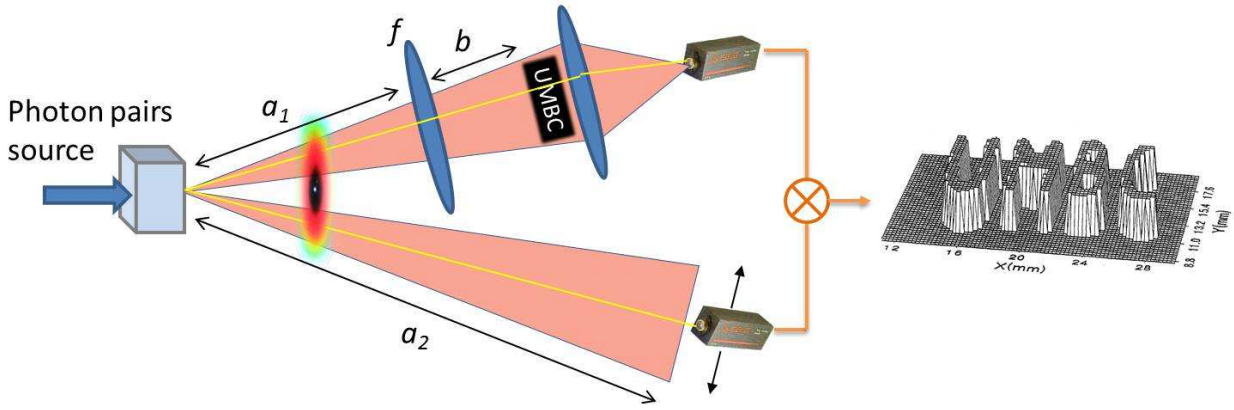


FIG. 1: Simplified illustration of the original ghost imaging experiment [11]. A mask with letters "UMBC" is placed in the object channel, where all light is collected by a "bucket detector". Nonetheless, an image is reconstructed by correlating this detector's photo counts with those from another detector, raster-scanning the *empty* reference channel. A sharp image is observed when a modified thin lens equation is fulfilled: $1/(a_1 + a_2) + 1/b = 1/f$.

reference channel. This could be convenient for imaging of hard-to-access objects. The ghost imaging is especially beneficial for imaging the objects at "inconvenient" wavelengths, such as far infrared, while the reference channel wavelength is visible [8]. Furthermore, the coincidence measurement technique is more robust in the presence of the optical background illumination. Finally, the possibility of surpassing the diffraction limit in ghost imaging has been discussed. However here one should be careful to acknowledge that while the transverse intensity correlation of parametric photons is not constrained by by the signal or idler wavelength diffraction, it is constrained by the pump wavelength diffraction.

Despite the apparent potential advantages, the first realization of ghost imaging was extremely far from any practical applications, and especially from astronomy. Indeed, the need for a laser-pumped source of photon pairs and the requirement to collect all light in the object channel (which means that the object has to be placed immediately before the collection optics) effectively ruled out such applications.

A first step towards practical ghost imaging was made ten years after its initial demonstration, when it was shown that the two-photon correlation properties of common thermal light are applicable for ghost imaging [13, 14]. Since thermal light sources are much more abundant than parametric light sources, and in particular in space, this realization was very important. Next, it was shown that collecting all the light in the object channel (the "bucket detection") is not required, and that some portion of scattered light could be collected instead [10]. This has allowed the object to be placed at a large distance from the observer. Remarkably, the approach by [10] has already relied on the (pseudo)thermal light source rather than on parametric light, as shown in Fig. 2.

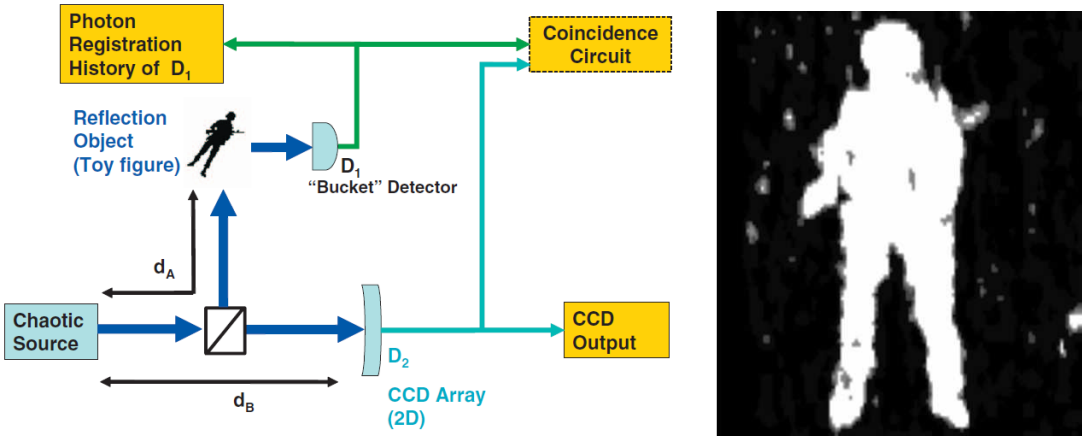


FIG. 2: Using a thermal light source with a point-like detector collecting the light scattered by an object gives access to ghost imaging of distant and hard to access objects. Experimental diagram and image from [10].

However, using thermal light sources brings about a new complication: a beam splitter that has to be placed between the source and the object (see Fig. 2). This beam splitter is needed to create the reference channel whose speckle pattern duplicates that in the object channel, enabling the intensity correlation imaging. Such a geometry can be easily implemented in a lab, but becomes problematic when both the source and object are located far in space.

In this work we address this problem. Our approach is illustrated in Fig. 3. The underlying idea of our approach is that an object that partially transmits and partially reflects or scatters light, can itself play the role of the beam splitter. Moreover, even a perfectly opaque (but not black) scattering object may under certain conditions (as discussed below) create coherence between the transmitted and scattered light, which may be utilized for the intensity correlation imaging. Since the object is present in both channels, this approach leads us away from "canonical" ghost imaging towards intensity interferometry of Hanbury Brown - Twiss type. The analogy and distinctions between these two types of imaging have been discussed in literature [15]. In our case, an important distinction is that we will not be concerned with the angular size or other properties of the source, which will be assumed to be known. Instead, we will study the effect of the object's geometry and location relative to the source and observer on the intensity correlation. We will attempt to restore these parameters from the correlation measurements and show that these results could provide important information in addition to conventional direct observations.

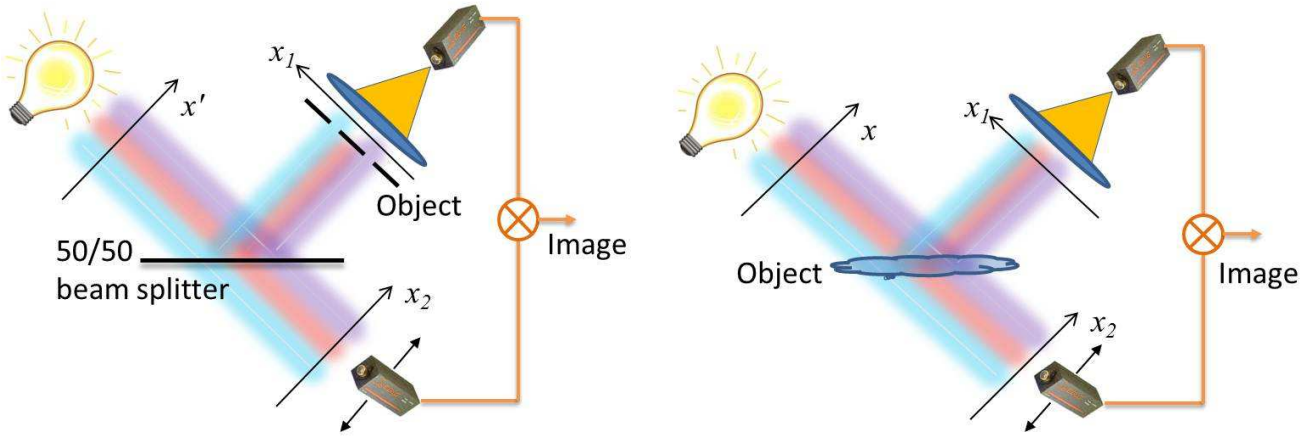


FIG. 3: Conceptual schematic of conventional thermal light ghost imaging setup (a) and of our approach (b)).

Configuration shown in Fig. 3(b) can be realized in three different ways, depending on whether one, both or none of the detectors see the direct light from the source in addition to the object-scattered light. Obviously, blocking one or both detectors from the direct light provides reduced background signal and appears advantageous. However, it requires the source and object to be optically resolvable and either mayrequire placing one or both detectors in space far apart from each other, or may not be feasible at all (for distant objects). In the following analysis we will assume both detectors to see the direct as well as scattered (in the nearly forward direction) light. Configurations when for one or both detectors the source can be blocked will simplify the the analysis. Below we will develop and test a simple analytical model that will allow us to study the intensity-correlation signatures of the simplest test objects. Based on this model we will make predictions concerning the observability of various space objects, and concerning their parameters that can be inferred from such observations.

Potential benefits of our approach are expected to include new capabilities for enhanced resolution, faint object detection, and broader range imaging of extra-terrestrial objects, such as Earth-like planets (including those near bright stars), black holes, dust or gas clouds. Further technical benefits include relaxed requirements for the space-based telescope quality and performance, as this telescope is effectively a "bucked detector" that does not require high spatial resolution. The enhanced spatial resolution is determined by a large baseline between the two detectors, in a way similar to the synthetic aperture approach. Optical imaging in astronomy will remain an active area of NASA's deep space exploration efforts for many years to come, and developing a novel architecture geared to provide new or enhanced data will definitely have a high impact. We expect the emergence of new research programs and space missions enabled by the technology we currently develop. The ramifications of this technology implementation extend beyond the scope of astronomy and astrophysics. Ghost imaging, of remote objects or of objects with limited access, attracts increasing attention from the military and national security agencies. JPL is presently involved in a DARPA project, managed by Dr. Erkmen, to investigate the applicability of ghost imaging for active remote-sensing instruments. In this task it has been shown that a recent innovation inspired by ghost imaging, named *computational ghost imaging* for its use of active modulation of a laser source with a spatial-light modulator in conjunction with post-

processing to derive an image of the target, is indeed a feasible remote sensing instrument for certain standoff-sensing scenarios [16, 17].

## III. THE RESEARCH PLAN AND ACCOMPLISHMENTS FOR THE PHASE I

The research plan of our Phase I effort is determined by the Phase I primer objective, which is to evaluate the feasibility of our approach at a conceptual level. This feasibility study is necessary because the geometry of "conventional" ghost imaging requires close access to either the object, or the light source, which makes astronomical applications difficult. In addition to solving this problem, we investigate the possibility of the next step, which would be to remove the optical beam splitter, which so far has been an indispensable part of ghost imaging with thermal light. In our approach the object itself takes on the function of the beam splitter. If successful, this approach will allow for real-world application of the correlation imaging technique, even for the astronomical observations. This distinguishes our proposal from other research presently carried out in the ghost imaging area. While the earlier study of ghost imaging provides solid theoretical base for the underlying approach, a thorough feasibility study is required prior to launching a large-scale effort focused on astronomy and astrophysics applications. The main goal of the 1-year Phase I has been to carry out such a study and present our recommendations by the Phase II start, as to whether such an effort would be practical at the present or near future level of technology. Three key questions were posed to be answered by this research:

1. Is the proposed approach feasible at a fundamental level?

2. What are the key quantitative advantages or value added to the conventional approaches?

3. What is an example of the conceptual architecture?

To achieve this goal we had proposed to complete the theoretical analysis of the base ghost imaging configuration as shown in Fig. 3(b). This analysis then would be used to provide the theoretical estimates of the technique's expected performance with respect to astronomical objects of interest. Based on these estimates, we had planed to discuss the practical aspects of ghost imaging in space, such as the signal to noise ratio (SNR), optical bandwidth, clock synchronization requirements, and others, to evaluate the advantages or establish the added benefits of the correlation imaging technique.

To gain confidence in our theoretical estimations, it is highly desirable to compare them to the available experimental observations. It is even more desirable to be able to carry out an experiment specifically designed to test our theoretical predictions. For this purpose we had included the design a bench-top experiment in our Phase I research program. This experiment is scheduled for the Phase II and is planned to mimic the astronomic observation following the observation scenario developed in Phase I.

The above Phase I research plan has been condensed into list of milestones (also available in the initial Phase I proposal) summarized below with a brief account of the accomplishments. The results needed more extended presentation are discussed in the following Sections.

1. **Complete the theoretical analysis of the astronomical ghost imaging baseline architecture.** Our analysis involving the model object and simple paraxial planar geometry is presented in Sections IV - VI below. It provides a definite positive answer to the key question (1) listed above.

2. **Develop the theoretical analysis of the astronomical ghost imaging advanced architecture.** Comparison of the results obtained from our simplified analytical model with an actual astronomical observation (the Kepler mission, see Section V) is encouraging and suggestive of deeper analysis, primarily concerned with comparison of the SNR of the traditional and innovative approaches. In its base form, such analysis is given in Section VII, while the relevant issues of spectral filtering and clock synchronization are discussed in Section IV. We conclude that while the correlation imaging cannot be considered for replacing the conventional intensity based imaging, it has a good potential for being its valuable upgrade capable of providing complimentary information, which essentially answers the key question (2) above. However this topic requires further and deeper investigation, which is incorporated in the Phase II task plan.

3. **Design of the proof-of-concept experiment.** The relevant literature has been reviewed. It has been decided that future experiment baseline will follow the typical in the field approach by [14, 18, 19] involving a pseudo-thermal light source and either a photon-counting or analogue photocurrents multiplication circuit. The PI has visited the authors of [18, 19] at MPL Erlangen, in Germany, and discussed the experimental details. These discussions are planned to continue. In particular, we are discussing the possible visit of one of the authors to

Caltech and JPL. The experimental demonstration of correlation imaging of phase and amplitude test object has been incorporated in the Phase II task plan.

4. **Provide recommendations for the follow-on research.** These recommendation, including the proposed future missions architectures (the answer to the key question (3) above), have been included into now awarded Phase II task plan, as outlined in Section VIII.

5. **Publish and present the research results at conferences.** Besides the NIAC symposia, the Ghost imaging of space objects research has been presented at the 21th International Laser Physics Workshop, in Calgary, Canada, July 23-27 2012, as an invited presentation. The PI has also been invited to give a lecture on this topic at the Max Plank Institute of Physics of Light (MPL Erlangen, Germany) annual retreat in October 8-12, 2012. The research results have been submitted to NASA's Interplanetary Network Progress Reports. Presently, we are working on the paper to be submitted to Open Access Journal of Physics. A no-cost extension of the Phase I effort has been granted to allow us to prepare this publication as part of the Phase I research.

## IV. 2D SOURCE AND OBJECT MODEL IN PARAXIAL APPROXIMATION

Let us consider a flat source and a flat object placed in the source and object planes where we introduce the local transverse coordinates $\vec{\rho}$ and $\vec{\rho_o}$, respectively. Let $L_s$ be the distance between the source and object planes, and $L_{1,2}$ the distances between the object plane and the planes of point-like detectors 1 and 2. The local transverse positions of these detectors are $\vec{\rho_1}$ and $\vec{\rho_2}$, respectively, as shown in Fig. 4.

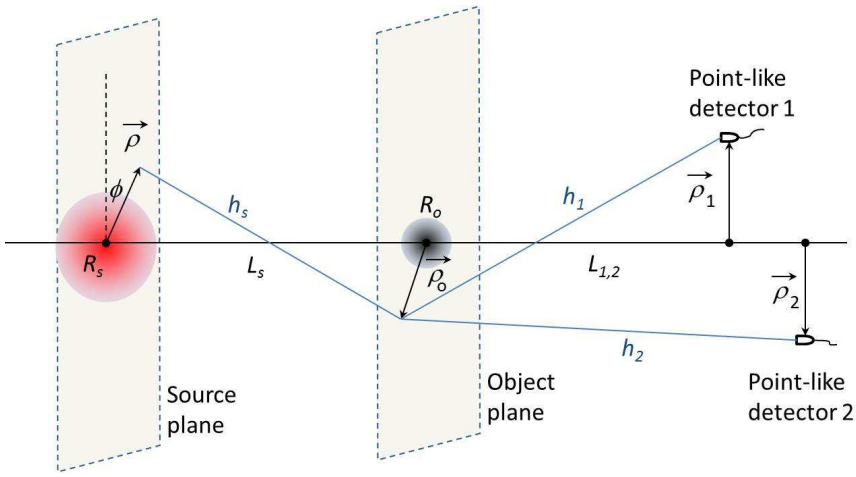


FIG. 4: Relative position of the source, object and detectors in the flat paraxial model.

Let us assume that the source field is bound by a Gaussian envelope with the width $R_s$ and can be written as $E(\vec{\rho}, t)e^{-\frac{\rho^2}{2R_s^2}}$. This model approximates the source with a diameter (intensity distribution FWHM) equal to $\sqrt{2}R_s$. In the paraxial approximation, the field at detector 1 is related to the field of the source as the following:

$$E_1(\vec{\rho_1}, t) = \int\int d^2\rho d^2\rho_o e^{-\frac{\rho^2}{2R_s^2}} E(\vec{\rho}, t - \frac{L_1 + L_s}{c}) h_{L_s}(\vec{\rho} - \vec{\rho_o}) T(\vec{\rho_o}) h_{L_1}(\vec{\rho_o} - \vec{\rho_1}), \tag{1}$$

where

$$h_Z(\vec{x}) = \frac{e^{ikZ}}{i\lambda Z} e^{ik\frac{|\vec{x}|^2}{2Z}} \tag{2}$$

is the field propagation function for the distance $Z$ and the transverse displacement $\vec{x}$ in the paraxial approximation, and $T(\vec{\rho_o})$ is a transmission function of the flat object. This transmission function may be real (purely absorbing object), imaginary (purely phase object, e.g. a thin lens) or complex. A similar to (1) relation can be written for the field at the other detector.

Let us consider the correlation-based ghost imaging. In this case the observable is

$$\langle I_1(\vec{\rho_1}, t_1) I_2(\vec{\rho_2}, t_2)\rangle \propto \langle E_1^\dagger(\vec{\rho_1}, t_1) E_2^\dagger(\vec{\rho_2}, t_2) E_1(\vec{\rho_1}, t_1) E_2(\vec{\rho_2}, t_2)\rangle. \tag{3}$$

For thermal light, the phase-sensitive term in (3) vanishes [17], and we arrive at

$$\langle I_1(\vec{\rho}_1,t_1)I_2(\vec{\rho}_2,t_2)\rangle \propto |\langle E_1^\dagger(\vec{\rho}_1,t_1)E_2(\vec{\rho}_2,t_2)\rangle|^2 + \langle E_1^\dagger(\vec{\rho}_1,t_1)E_1(\vec{\rho}_1,t_1)\rangle\langle E_2^\dagger(\vec{\rho}_2,t_2)E_2(\vec{\rho}_2,t_2)\rangle, \tag{4}$$

where the first term describes the possible ghost image and the second term gives the uncorrelated "background" intensity product, which also describes the object's shadow. To separate these effects it is convenient to introduce the normalized Glauber correlation function [20]

$$g^{(2)}(\vec{\rho}_1,t_1;\vec{\rho}_2,t_2) = 1 + \frac{|\langle E_1^\dagger(\vec{\rho}_1,t_1)E_2(\vec{\rho}_2,t_2)\rangle|^2}{\langle E_1^\dagger(\vec{\rho}_1,t_1)E_1(\vec{\rho}_1,t_1)\rangle\langle E_2^\dagger(\vec{\rho}_2,t_2)E_2(\vec{\rho}_2,t_2)\rangle} = 1 + \frac{|G_{12}|^2}{G_{11}G_{12}}. \tag{5}$$

Glauber correlation function will be our main observable in the following treatment. However let us mention that other types of measurements are possible. In particular, one can measure higher-order correlation functions $g^{(m,n)}$, or the variance of intensity difference (rather than a product) [18, 19, 21]. The analysis based on the field propagation equation (1) can be easily extended to these measurements. Such measurements will have different dependencies on the optical mode structure and on the detector's quantum efficiencies, and may offer interesting resolution-SNR trade-off opportunities. The possibility of utilizing these measurement strategies distinguished our approach from the conventional intensity interferometry.

Substituting the fields $E_1(\vec{\rho}_1,t_1)$ and $E_2(\vec{\rho}_2,t_2)$ given by (1) into (5) we take into account the correlation property of the source field $E(\vec{\rho},t)$

$$\langle E^\dagger(\vec{\rho},t)E(\vec{\rho'},t')\rangle \propto \delta(\vec{\rho}-\vec{\rho'})\Gamma(t-t'), \tag{6}$$

where $\Gamma$ is a $\delta$-like function whose width corresponds to the optical coherence time. The latter may be determined by the spectral filters bandwidth. Unless we are interested in color imaging, using narrow-band filters is undesirable because they reduce the signal. On the other hand, short coherence time requires compatibly fast optical detectors and correlation circuitry, in order to ensure single longitudinal mode detection. Therefore to carry out a fair comparison between the direct intensity measurement and the correlation measurement, we need to take into account the photon flux reduction due to the minimal spectral filtering, required in the latter case. Let us assume a 1 ps timing accuracy and the central wavelength of 1 micron. This accuracy requirement may appear stringent, as most contemporary time-stamp systems have time resolution below 50 ps, while the pulse front jitter in commercial photon counting detectors can be as low as 30 ps. However these state of the art figures show strong improving trends. Projecting these trends, it is reasonable to expect a single-digit picasecond time resolution systems available by the time our concept matures.

A 1 ps coherence time corresponds to a 3.3 nm wide spectral band around 1 micron central wavelength. Comparing the optical power detected within this band to the total power within the typical band of a silicon photo detector (see Fig. 5) we find the for a correlation measurement we have 0.5% of the power in our disposal than for the broad-band intensity measurement. This reduces the signal to noise ratio (SNR) in a shot-noise limited narrow-band measurement. The relative SNR will be more favorable for the correlation measurement when compared to a color-resolved intensity measurement. In particular, no flux loss will be suffered if one is interested in a very narrow-band measurement, e.g. a measurement with a specific spectral line. A more detailed discussion of the direct-intensity vs. correlation measurement SNRs will be given below in Section VII.

Let us point out that in addition to the high speed and low jitter requirements on the photo detectors and correlation electronics, a the broad-band correlation measurement placed stringent requirements on the clock synchronization between the two detectors, as well as on the knowledge of their relative position $L_1 - L_2$. Recent spectacular breakthrough in the field of ultra-precise clocks (in particular, optical clocks) has created a powerful stimulus to development adequate time transfer protocols. A tremendous progress has been made in this area during the recent years. Synchronization of a pair of stationary clocks down to the required precision is already within reach. More difficulties arise in case of a space-based observer(s). Then the clock synchronization problem is inseparable from the ranging problem, which, in our example of 1 ps timing accuracy, should be as good as 30 microns. This problem also has a solution. As one example, in the on-going GRAIL mission Ka-band ranging allows for the 10 microns ranging error. Even more accurate ranging is required and being developed for the optical VLBI and synthetic aperture applications, such as LISA. We expect to be able to leverage this technology which may be expected to advance even further by the time of the "Ghost imaging of space objects" mission design.

As an alternative, the time synchronization problem can be considerably alleviated if one takes the advantage of the fact that in our approach we always rely on the maximum correlation, that is, zero delay between the photon arrival times. This will allow us to continuously "tweak" the local clocks so as to maximize the measured correlation function, and to monitor that change of this maximal value. In a sense, this would amount to using the detected signal as a time-synchronization signal; an approach one might call a "stellar GPS".

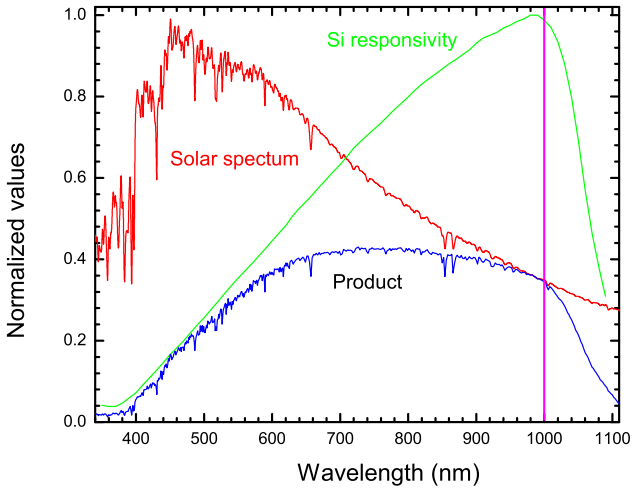


FIG. 5: The solar radiation normalized spectral density (from [22]), spectral sensitivity of a typical silicon photo diode, and their product.

To continue our analysis we will assume that perfect synchronization between the detectors has been achieved and $\Gamma(t-t')=1$ in (6). We then suppress the temporal part of the problem. For the numerator in (5) we derive

$$G_{12}(\vec{\rho_1},\vec{\rho_2}) = \int\int\int d^2\rho d^2\rho_o' d^2\rho_o \; e^{-\frac{\rho^2}{R_s^2}} T_2(\vec{\rho_o}) T_1^*(\vec{\rho_o'}) \; h_{L_s}^*(\vec{\rho}-\vec{\rho_o'}) h_{L_s}(\vec{\rho}-\vec{\rho_o}) h_{L_1}^*(\vec{\rho_o'}-\vec{\rho_1}) h_{L_2}(\vec{\rho_o}-\vec{\rho_2}). \tag{7}$$

In (7) we have introduced $T_{1,2}(\vec{\rho_o})$ to allow the transmission functions to be different for detectors 1 and 2. This will allow us to consider the scenario when the object (partially) obscures the source light for one detector, and scatters it to the other. That is, the former detector receives the direct light from the source, but the latter only sees the light scattered by the object. In handling such situations we still need to make sure the paraxial approximation holds, and that the approximation of a flat object remains reasonable.

For the following analysis it will be convenient to introduce a correlation function

$$G_{12}^{(R_s)}(Z_a,\vec{\rho}_a;Z_b,\vec{\rho}_b) = \int d^2\rho e^{-\frac{\rho^2}{R_s^2}} h_{Z_a}^*(\vec{\rho}-\vec{\rho_a}) h_{Z_b}(\vec{\rho}-\vec{\rho_b}) \tag{8}$$

for the fields emitted by an extended Gaussian source of thermal light that has a width $R_s$ and is located at $Z=0$, propagating to locations $(Z_a,\vec{\rho}_a)$ and $(Z_b,\vec{\rho}_b)$. Equivalently, from the *advanced wave* perspective [23], it describes time-reversed propagation of a photon from $(-Z_a,\vec{\rho}_a)$ to the source, and then forward in time to $(Z_b,\vec{\rho}_b)$. If the source is infinitely large, $R_s\to\infty$, the aperture-limited propagation function (8) becomes equal to a point-source propagation function from one detector to the other:

$$G_{12}^{(\infty)}(Z_a,\vec{\rho}_a;Z_b,\vec{\rho}_b) = h_{Z_b-Z_a}(\vec{\rho}_b-\vec{\rho}_a). \tag{9}$$

The two-point propagation function arises in (5):

$$G_{12}(\vec{\rho_1},\vec{\rho_2}) = \int\int d^2\rho_o d^2\rho_o' h_{L_2}(\vec{\rho_o}-\vec{\rho_2}) h_{L_1}^*(\vec{\rho_o'}-\vec{\rho_1}) T_2(\vec{\rho_o}) T_1^*(\vec{\rho_o'}) G_{12}^{(R_s)}(L_s,\vec{\rho_o'};L_s,\vec{\rho_o}), \tag{10}$$

and likewise for $G_{11}(\vec{\rho_1})$ and $G_{22}(\vec{\rho_2})$. To evaluate $G_{12}^{(R_s)}(Z_a,\vec{\rho}_a;Z_b,\vec{\rho}_b)$ in a general form we introduce polar coordinates such that

$$\int d^2\rho = \int_0^\infty \rho d\rho \int_0^{2\pi} d\varphi, \quad |\vec{\rho_a}-\vec{\rho_b}|^2 = \rho_a^2+\rho_b^2-2\rho_a\rho_b\cos(\varphi_a-\varphi_b). \tag{11}$$

The angular integration in Eq. (8) yields

$$G_{12}^{(R_s)}(Z_a,\vec{\rho}_a;Z_b,\vec{\rho}_b) = 2\pi\frac{e^{ik(Z_b-Z_a)}}{\lambda^2 Z_a Z_b} \; e^{i\frac{k}{2}(\rho_b^2/Z_b-\rho_a^2/Z_a)} \int_0^\infty \rho d\rho e^{-\rho^2\left[\frac{1}{R_s^2}+ik\frac{Z_b-Z_a}{2Z_aZ_b}\right]} \; J_0\left(k\rho\left|\frac{\vec{\rho}_b}{Z_b}-\frac{\vec{\rho}_a}{Z_a}\right|\right). \tag{12}$$

Then integrating over the radius we obtain

$$G_{12}^{(R_s)}(Z_a,\vec{\rho}_a;Z_b,\vec{\rho}_b)=2\pi\frac{R_s^2}{\lambda^2}\frac{e^{ik(Z_b-Z_a)}}{2Z_aZ_b+ikR_s^2(Z_b-Z_a)}\,e^{i\frac{k}{2}(\rho_b^2/Z_b-\rho_a^2/Z_a)}e^{-\frac{k^2}{2}\left|\frac{\vec{\rho}_b}{Z_b}-\frac{\vec{\rho}_a}{Z_a}\right|^2\frac{R_s^2Z_aZ_b}{2Z_aZ_b+ikR_s^2(Z_b-Z_a)}}. \tag{13}$$

In the case of interest (10) we have $Z_a=Z_b=L_s$, which leads to

$$G_{12}^{(R_s)}(L_s,\vec{\rho_o'};L_s,\vec{\rho_o})=q^2\pi^{-1}e^{i\frac{q}{R_s}(\rho_o^2-\rho_o'^2)}e^{-q^2\left|\vec{\rho_o}-\vec{\rho_o'}\right|^2}, \tag{14}$$

where $q^{-1}=2L_s/(kR_s)$ is the speckle size.

## V. BALANCED ARMS CONFIGURATION

In this section we consider the balanced case when $L_1=L_2=L$. While this case limits possible observation scenario, it allows us to carry out exact analytical calculations in many cases of interest, and to asses the practical utility of our approach. To carry out these calculation it will be convenient to introduce the new coordinates $\vec{x}=(\vec{\rho_o}+\vec{\rho_o'})/\sqrt{2}$ and $\vec{y}=(\vec{\rho_o}-\vec{\rho_o'})/\sqrt{2}$. Then substituting (14) into (10) we obtain

$$G_{12}(\vec{\rho_1},\vec{\rho_2})=A\int\int S(\vec{x},\vec{y})e^{-2q^2y^2}e^{i\vec{\Delta}\vec{x}}e^{i\vec{\Sigma}\vec{y}}e^{i\gamma\vec{x}\vec{y}}d^2xd^2y, \tag{15}$$

where

$$\begin{aligned}
A &= \pi\left(\frac{R_s}{\lambda^2LL_s}\right)^2 e^{\frac{ik}{2L}(\rho_2^2-\rho_1^2)},\\
S(\vec{x},\vec{y}) &= T_2(\frac{\vec{x}+\vec{y}}{\sqrt{2}})T_1^*(\frac{\vec{x}-\vec{y}}{\sqrt{2}}),\\
\vec{\Delta} &= \frac{k}{\sqrt{2}L}(\vec{\rho}_1-\vec{\rho}_2),\\
\vec{\Sigma} &= \frac{k}{\sqrt{2}L}(\vec{\rho}_1+\vec{\rho}_2),\\
\gamma &= k(1/L+1/L_s).
\end{aligned} \tag{16}$$

The Gaussian term in (15) arises from Fourier transform of the source field distribution. This suggests that (15) could be generalized for any such distribution. However at this stage we will limit our consideration to a Gaussian source.

As a sanity check we notice that if we "turn off" the object by setting $S(\vec{x},\vec{y})=1$, the integral over $d^2x$ in (15) yields $(2\pi)^2\delta(\vec{\Delta}+\gamma\vec{y})$. Then the $d^2y$ integral yields, quite expectedly, the correlation function of a Gaussian source (14) with increased free-space propagation length $L_s\to L+L_s$:

$$G_{12}(\vec{\rho_1},\vec{\rho_2})\to G_{12}^{(R_s)}(L+L_s,\vec{\rho}_1;L+L_s,\vec{\rho}_2). \tag{17}$$

Let us now consider a few example objects and discuss their possible relevance for the astronomy applications.

### A. A Gaussian absorber.

This case can represent e.g. a spherical dust or gas cloud of roughly uniform density. It also can be used as a crude model for a planet occluding a star. The transmission function of such an object can be modeled as

$$T(\vec{\rho}_o)=1-T_0e^{-\frac{\rho_o^2}{2R_o^2}}, \tag{18}$$

which gives rise to four terms:

$$S(\vec{x},\vec{y})=S_0+S_{1a}+S_{1b}+S_2=1-T_0e^{-\frac{(\vec{x}+\vec{y})^2}{4R_o^2}}-T_0e^{-\frac{(\vec{x}-\vec{y})^2}{4R_o^2}}+T_0^2e^{-\frac{x^2+y^2}{2R_o^2}}. \tag{19}$$

In (18) and (19) $T_0$ is the amplitude transmission of the most opaque (central) part of the object. Consequently, the correlation function also will consist of four terms: $G_{12}=G_{12}^{(0)}+G_{12}^{(1a)}+G_{12}^{(1b)}+G_{12}^{(2)}$, where the zero-order term

corresponds to free-space propagation (17): $G_{12}^{(0)} = G_{12}^{(R_s)}(L+L_s, \vec{\rho}_1; L+L_s, \vec{\rho}_2)$. A straightforward but cumbersome calculations gives both the first and the second order terms in the form

$$G_{12}^{(1,2)}(\vec{\rho}_1, \vec{\rho}_2) = \frac{(-T_0)^n}{\pi(\tilde{q}^2 + R_o^2\tilde{\gamma}^2)} \left(\frac{k^2 R_s R_o}{2LL_s}\right)^2 e^{-i\frac{k^2 R_o^2 \tilde{\gamma}}{2L^2}\frac{\rho_2^2-\rho_1^2}{\tilde{q}^2+R_o^2\tilde{\gamma}^2}} e^{-\frac{k^2(\vec{\rho}_2+\vec{\rho}_1)^2}{8L^2(\tilde{q}^2+R_o^2\tilde{\gamma}^2)}} e^{-\frac{k^2 R_o^2 \tilde{q}^2}{2L^2}\frac{(\vec{\rho}_2-\vec{\rho}_1)^2}{\tilde{q}^2+R_o^2\tilde{\gamma}^2}}. \tag{20}$$

To obtain $G_{12}^{(1a,b)}$, we substitute in (20)

$$n = 1, \quad \tilde{q}^2 = 2q^2 + \frac{1}{4R_o^2}, \quad \tilde{\gamma} = \gamma \pm \frac{i}{2R_o^2}.$$

For $G_{12}^{(2)}$, we substitute

$$n = 2, \quad \tilde{q}^2 = 2q^2 + \frac{1}{2R_o^2}, \quad \tilde{\gamma} = \gamma.$$

We notice that in the multi-mode case when the speckle size on the object greatly exceeds the object size, $\tilde{q}^2 \approx 2q^2$. However we do not need to make this approximation now.

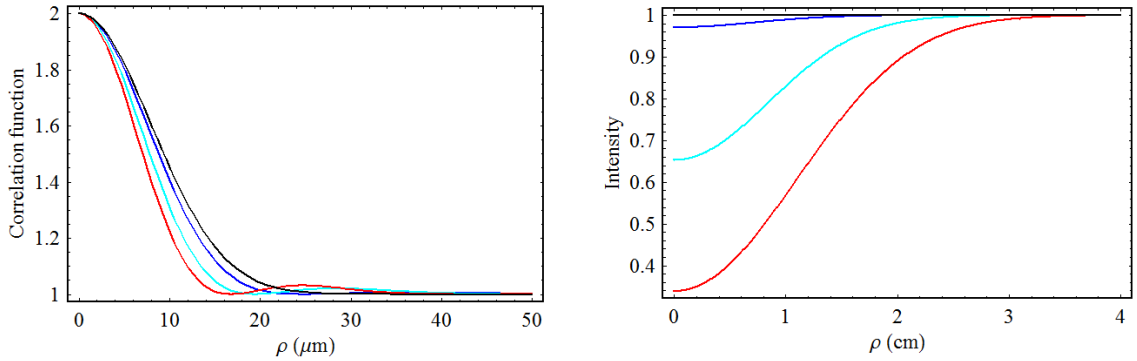


FIG. 6: The correlation function $g^{(2)}(\vec{\rho}_1 = -\vec{\rho}_2)$ (on the left) and the intensity profile (on the right) for $T_0 = 1$, $L_s = L = 50$cm and $R_s = 1$cm. The object size $R_o$ is varied from zero (no shadow, largest speckle) to 1, 2 and 3 mm (deepest shadow, smallest speckle).

In Fig. 6 we show a correlation function $g^{(2)}(\vec{\rho}_1 = -\vec{\rho}_2)$ (on the left) and the intensity profile featuring the object's shadow (on the right). In this simulation the opaque ($T_0 = 1$) object is placed between the source ($R_s = 1$ cm) and the detectors plane so that $L_s = L = 50$ cm. The object size $R_o$ is varied from zero to 1, 2 and 3 mm. As the object becomes larger its shadow becomes deeper and (less intuitively) the speckle size becomes smaller and acquires a structure. Even less intuitive evolution is undergone by the speckle size as the object is moved across the line of sight imitating a planet passing across the star. The speckle first gets broader, and then narrower, reaching the minimum when the object is exactly on the line of sight, see Fig. 7. To simulate this transient we actually changed the detector's position $(\rho_1 + \rho_2)/2$ while the $R_o = 3$ mm object was fixed on the initial line of sight at $L_s = L = 50$ cm. In Fig. 7 we show the corresponding variation of the speckle width and the normalized intensity received by the detectors.

Let us apply our model to an actual astronomical observation carried out at Kepler space telescope [1, 2]. Substituting in our model the Kepler-20f parameters [2] we find the relative intensity variation of the order of $10^{-4}$, which is consistent with the actual observation [2], see Fig. 8. The disagreement in the dip shape arises from using the Gaussian absorber model while the actual planet is, of course, better described by an opaque disk. However the numerical agreement with the experiment shows that even a simplistic fully analytical Gaussian model can be useful. Following this model we predict the variation of the speckle size from 3.6091 km when the planet is out of the line of sight to 3.6086 km when it it in the line of sight, which corresponds to the relative variation of $1.4 \times 10^{-4}$. Remarkably, the magnitude of this variation is very close to the magnitude of the photon flux variation. Of course, a detailed SNR analysis is required in order to conclude which type of planetary detection will be more efficient. Let us however point out that the measurement of the speckle width does not preclude the conventional intensity measurement, such as has been carried out in the Kepler experiment, and can be considered as an *extension of such a measurement rather than its substitute.*

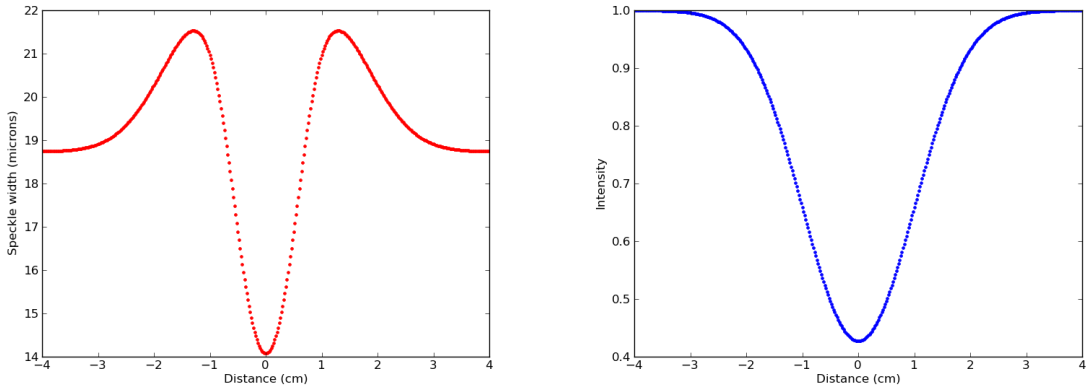


FIG. 7: Width of the correlation function $g^{(2)}(\vec{\rho}_1 = -\vec{\rho}_2)$ (on the left) and the intensity (on the right) dependence on displacement of the detectors from the line of sight.

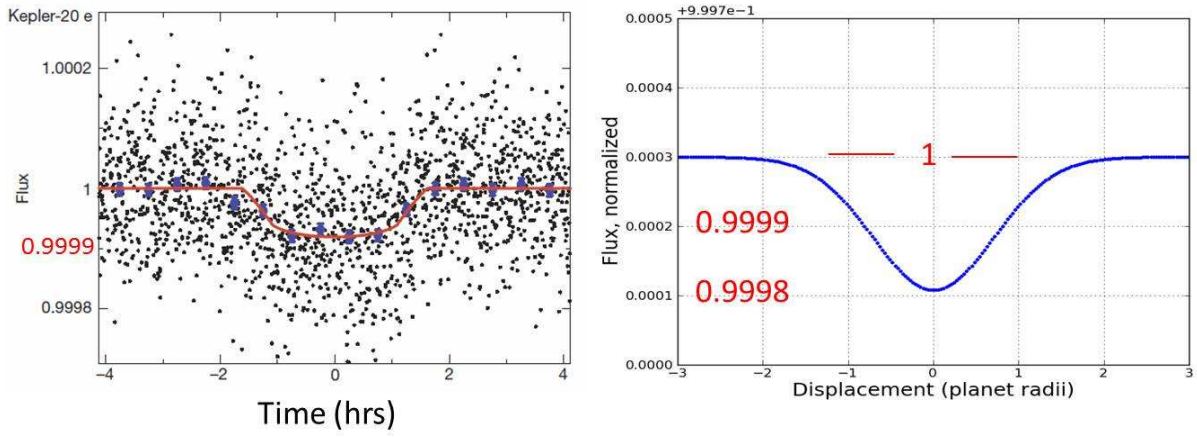


FIG. 8: The intensity variation for Kepler-20e observed in [2] (on the left) and computed based on our model (on the right).

### B. Phase objects.

Let us consider another model object allowing for the fully analytical treatment: a thin lens. The motivation for studying of this example is the possibility to observe purely phase object where direct intensity measurements may not be as efficient as with opaque objects. Examples of such objects in space may be gravitational lenses or dilute gas clouds. For an infinite thin lens with focal distance $f$,

$$S(\vec{x},\vec{y}) = e^{-\frac{ik}{2f}(\rho_o^2-\rho_o'^2)} = e^{-i\frac{k}{f}\vec{x}\vec{y}}. \tag{21}$$

The effect of such a lens can be absorbed into $\gamma \to \gamma_f = k(1/L + 1/L_s - 1/f)$, and we quickly arrive to

$$\begin{aligned} G_{11} = G_{22} &= \frac{q^2}{\pi D^2} = \text{const}|_{\vec{\rho}_{1,2}}, \\ G_{12}(\vec{\rho_1},\vec{\rho_2}) &= \frac{q^2}{\pi D^2}\, e^{\frac{ik}{2L}\frac{D-1}{D}(\rho_2^2-\rho_1^2)} e^{-(q/D)^2|\vec{\rho_2}-\vec{\rho_1}|^2}, \\ g_{12}(\vec{\rho_1},\vec{\rho_2}) &= 1 + e^{-2(q/D)^2|\vec{\rho_2}-\vec{\rho_1}|^2}, \end{aligned} \tag{22}$$

where $D \equiv L(1/L + 1/L_s - 1/f)$ is a dimensionless "out-of-focus" factor. If the lens images the source plane onto the detector plane then $D = 0$ and the speckles become infinitely small while the intensity goes to infinity. The former is a consequence of our assumption (6) of a delta-correlated source field. The latter is a consequence of the

paraxial approximation, as well as the coordinate-independent intensities in (22). If the source is in focus then the light propagates as a collimated beam, $D = 1$ and the speckle size as well as the intensity in the detector plane will be the same as in the lens plane.

Let us consider another example of a combined phase and amplitude lens-like object. This object has a finite extent and allows for the analytical treatment. Its transmission function is

$$T(\vec{\rho}_o) = 1 - e^{-\frac{\rho_o^2}{2R_o^2}}(1 - e^{-\frac{ik\rho_o^2}{2f}}). \tag{23}$$

This object can produce shadows very similar to those from a Gaussian absorber, see Fig. 9 (a) and (b). Therefore it would not be possible to distinguish these two objects based on the intensity measurement. However the behavior of the speckle widths is clearly distinct, as we see from Fig. 9 (c) and (d) (notice the difference in the signal magnitude, as well as in its character). This example demonstrate the potential the correlation measurement has for the object *characterization*, beyond its mere detection.

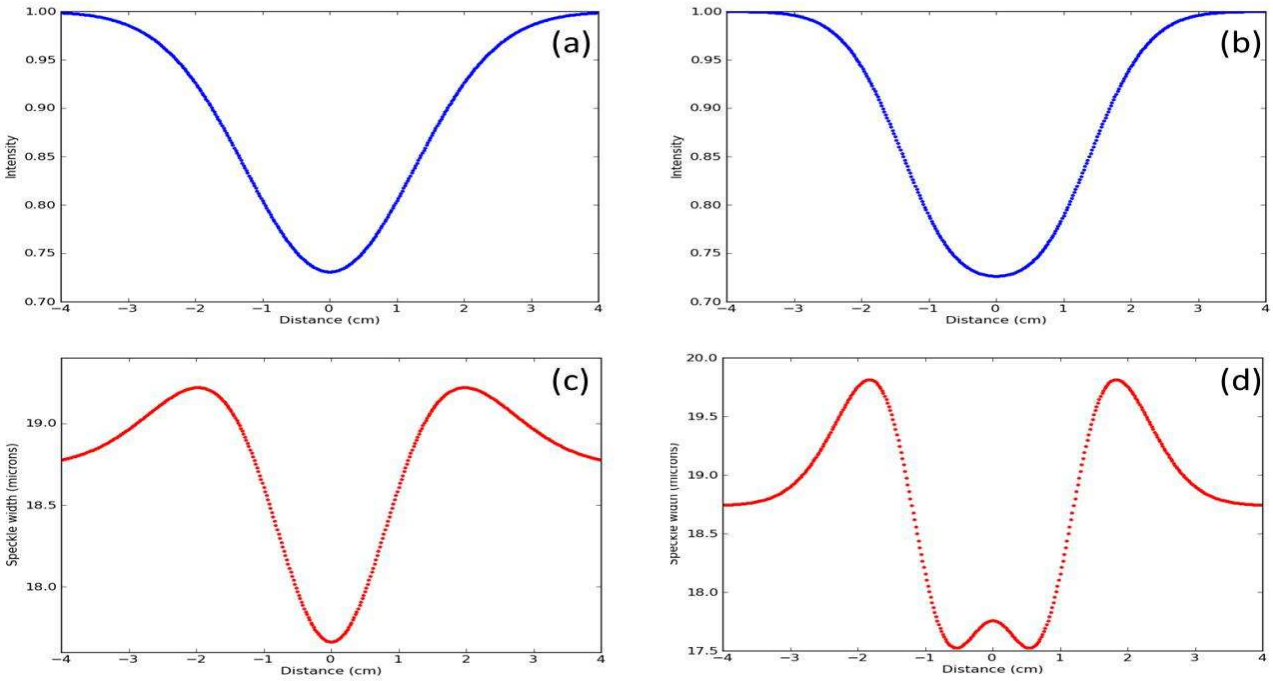


FIG. 9: (a): A shadow from a test object (23) with $R_o = 3$ mm and $f = 1$ m inserted between the source and detectors as a function of its position. (b) A shadow from a Gaussian absorber with $R_o = 5$ mm and $T_0 = 0.62$. (c) and (d): The speckle width for (a) and (b), respectively.

## VI. UNBALANCED ARMS CONFIGURATION

In this section we consider a more general case of $L_1 \neq L_2$ which may be important for an asymmetric configuration, e.g. when the correlation measurement is performed by a ground-based detector jointly with a distant space-based detector. We will continue to assume perfect time synchronization between the two detectors, or equivalently, a monochromatic light source. However we will not be able to carry out the analytical calculations without making some reasonable approximations. From (13) we see that the *large aperture approximation* (9) holds if

$$\alpha_s \equiv \frac{2Z_aZ_b}{kR_s^2|Z_b - Z_a|} \ll 1. \tag{24}$$

This approximation is appropriate for evaluation of the first-order terms in (10) where $Z_b - Z_a = L_1$ is large. Indeed, in this case for the optics lab geometry $\lambda = 1$ $\mu$m and $R_s = L_s = 1$ cm we get $\alpha_s = 1.6 \times 10^{-5}$. For the Solar system geometry with $R_s = 7 \times 10^5$ km (Sun radius), $L_s = 1.5 \times 10^8$ km (the distance from Earth to Sun), and $\lambda = 1$ $\mu$m, we get $\alpha_s = 5 \times 10^{-14}$. This parameter becomes even smaller for inter stellar distances. Therefore when we calculate

$G_{12}$ (10) for a Gaussian absorber described by (18), the first-order terms can be approximated as

$$G_{12}^{(1)}(\vec{\rho}_1,\vec{\rho}_2) \equiv G_{12}^{(1a)}(L_1,\vec{\rho}_1;L_2,\vec{\rho}_2) + G_{12}^{(1b)*}(L_2,\vec{\rho}_2;L_1,\vec{\rho}_1) \approx -2\int d^2\rho\, e^{-\frac{\rho^2}{2R_o^2}} h_{L_1}^*(\vec{\rho}-\vec{\rho}_1)h_{L_2}(\vec{\rho}-\vec{\rho}_2). \qquad (25)$$

The opposite case of (24) occurs when $Z_a = Z_b$. If furthermore $q^2$ is much greater than all coefficients that multiply $\rho^2$ in all real and imaginary exponents in (10), then (14) can be proven to approach a $\delta$-function normalized to unity. This is the *small aperture approximation*, applicable for the second-order terms of (10). Let us point out that within this approximation, the object cannot create coherence between the transmitted and scattered light unless the speckle size in the object plane approaches or exceeds the size of the object itself.

For the optics lab geometry as described above, $q^2$ exceeds all relevant parameters by a factor of at least $3\times10^4$. The excess factors are much greater in all reasonable astronomical geometries. Therefore we derive

$$G_{12}^{(2)}(\vec{\rho}_1,\vec{\rho}_2) \approx \int d^2\rho\, e^{-\frac{\rho^2}{R_o^2}} h_{L_1}^*(\vec{\rho}-\vec{\rho}_1)h_{L_2}(\vec{\rho}-\vec{\rho}_2). \qquad (26)$$

Therefore for a Gaussian absorber case with $L_1 \neq L_2$ we have the following approximate expressions:

$$\begin{aligned} G_{12}^{(0)}(\vec{\rho}_1,\vec{\rho}_2) &= G_{12}^{(R_s)}(L_1+L_s,\vec{\rho}_1;L_2+L_s,\vec{\rho}_2), \\ G_{12}^{(1)}(\vec{\rho}_1,\vec{\rho}_2) &= -2G_{12}^{(\sqrt{2}R_o)}(L_1,\vec{\rho}_1;L_2,\vec{\rho}_2), \\ G_{12}^{(2)}(\vec{\rho}_1,\vec{\rho}_2) &= G_{12}^{(R_o)}(L_1,\vec{\rho}_1;L_2,\vec{\rho}_2). \end{aligned} \qquad (27)$$

Let us first evaluate the correlation function $g^{(2)}$ found by substituting (27) into (5) in the absence of the object, by setting $R_o = 0$. In the left pane of Fig. 10 we show this function for a typical optical lab parameters ($L_1 \approx L_2 = 1$ m, $L_s = 1$ cm, $\lambda = 1$ $\mu$m), where we assumed that the detectors are coplanar with the line of sight and lie on its opposite sides: $\vec{\rho}_1 = -\vec{\rho}_2$. This allows us to use a single scalar parameter $\rho$, in the same way it was done in Fig. 6.

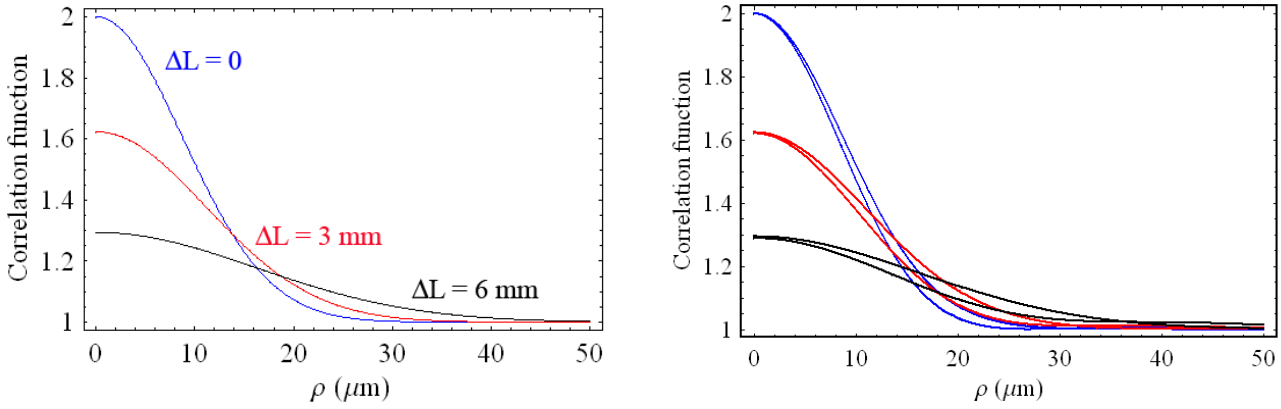


FIG. 10: Left: the correlation function $g^{(2)}(\vec{\rho}_1 = -\vec{\rho}_2)$ in the absence of an object for $R_s = 1$ cm $L_1 = 1$ m and $L_2 = L_1 + \Delta L$. Right: the speckles shown on the left become narrower when a small ($R_o = 1$ mm) Gaussian absorbing object is placed half the way between the source and detectors.

The correlation loss due to $\Delta L$ is clearly visible. We would like to emphasize that this is not due to a limited longitudinal coherence of the source, but because of its transverse coherence properties. We can interpret this result as following. By placing the first detector in the plane $L_1$ we define the speckle pattern in this plane as the transverse mode structure. These speckles may be further considered as mutually incoherent light sources. As light from these sources propagates further, the coherence areas expand as well as overlap. The expansion causes the widening of the correlation function while the overlap causes the contrast reduction due to multimode detection. Using the expression $g^{(2)}(0) = 1+1/m$ relating the correlation peak for thermal light to the number of detected modes $m$ we can determine that in our example the longitudinal displacement of the detector by $\Delta L = 6$ mm has lead to the number of detected modes $m \approx 3$. Note that this interpretation differs from the speckle pattern behavior that one might observe e.g. on a screen. In this case the speckle do not overlap and do not appreciably change in size for small longitudinal translations.

Now let us "turn on" the object and investigate its effect on the correlation function. If a small ($R_o = 1$ mm) object is placed half way between the source and the detectors, the correlation function becomes narrower, which means smaller speckles, see the right panel of Fig. 10.

Let us point out that the $\Delta L = 0$ case in Fig. 10 is consistent with the $R_o = 1$ mm case from Fig. 6, which validates the large-aperture and small-aperture approximations for an absorbing object. On the other hand, we notice that it fails for a phase object such as a thin large lens. When the small aperture approximation is utilized and (14) is treated as a $\delta$-function, such object is "erased" by taking the absolute-square of $T(\rho_o)$.

## VII. SIGNAL-TO-NOISE RATIO ANALYSIS

The sensitivity of the correlation-based measurements can be ascertained by a careful study of the signal-to-noise ratio, which strongly depends on the object of interest and the imaging geometry. As a result, the value added by the correlation-based measurement can range from significant to negligible. The quantitative analysis of the signal-to-noise ratio (SNR) for both types of measurements can leverage SNR calculations for Hanbury Brown-Twiss intensity interferometry, because performing ghost imaging in inter-galactic scales often yields geometries wherein the detectors are point-like (rather than bucket-like, which is more common in lab demonstrations of ghost imaging).

The ghost imaging configuration shown in Fig. 4 consists of two point-like detectors, each measuring the incident far-field irradiance resulting from the thermal source and object combination. The correlation of the two photocurrent outputs isolates the common irradiance fluctuations at their respective transverse locations, yielding information on the mutual coherence function of the effective source created by the true source illuminating the object.

Suppose the baseband envelope of the field incident on detector $m$, for $m = 1, 2$, is denoted by $E_m(t)$ for $0 < t < T$, having units $\sqrt{\text{photons/s}}$. Because we are considering thermal fields, we assume that have zero mean (i.e., $\langle E_m(t)\rangle = 0$) and a complex degree of coherence

$$\gamma_{1,2}(t-u) \equiv \frac{\langle E_1^*(t)E_2(u)\rangle}{\sqrt{\langle|E_1(t)|^2\rangle\langle|E_2(u)|^2\rangle}} \tag{28}$$

that is nonzero. We assume that the the coherence time of the two fields (i.e., the time delay $\tau$ for which $\langle E_m^*(t+\tau)E_m(t)\rangle$ is appreciable) is equal and given by $T_c$.

We will carry the following analysis for the photo currents $i_1(t)$ and $i_2(t)$ produced by the detectors in response to the incident optical field. This analysis can be easily generalized for the photon-counting detectors. We have

$$\langle i_m(t)|E_m(t)\rangle = \eta \int \mathrm{d}\tau\, |E_m(\tau)|^2 h_B(t-\tau)\,, \tag{29}$$

and

$$\langle \Delta i_m(t)\Delta i_m(u)|E_m(\cdot)\rangle = \eta \int \mathrm{d}\tau |E_m(\tau)|^2 h_B(t-\tau)h_B(u-\tau)\,. \tag{30}$$

Here $\Delta i(t) \equiv i(t) - \langle i(t)\rangle$, $h_B(t)$ denotes the real-valued baseband impulse response of the photodetectors with time constant (i.e., inverse bandwidth) equal to $T_B$. With little loss in generality, we assume that $\int \mathrm{d}t\, h_B(t) = 0$, i.e., that the photodetectors are DC blocking, and that $T_B \ll T_c$, i.e., that the coherence time of the source is much longer than the response time constant of the photo detector. Note that the DC term is useful for direct intensity observations, thus it could be tapped off prior to the $h_B(t)$ filter.

The equal-time photocurrent correlation measurement performed at the receiver corresponds to

$$C \equiv \int_0^T \mathrm{d}t\, i_1(t) i_2(t)\,, \tag{31}$$

where $C$ is repeated for every position of the two detectors. Thus, strictly speaking $E_m$, $i_m$ and $C$ should have two vector arguments indicating the positions of the two detectors in 2D or 3D space. However, here we are concerned with the SNR at a particular position of these detectors, and therefore we are omitting these variables to avoid clutter. The SNR of the $C$ measurement is defined then as

$$\text{SNR} \equiv \frac{\langle C\rangle}{\sqrt{\langle (C - \langle C\rangle)^2\rangle}}\,. \tag{32}$$

Calculating the first and second moments is tedious, but straightforward [17, 24]. The SNR can be evaluated, in the $T_c \gg T_B$ limit, as [24]

$$\text{SNR} = \frac{\sqrt{TT_B}}{T_c} \frac{|\gamma_{1,2}|^2 N}{\sqrt{1 + 2N(T_B/T_c) + N^2(T_B/T_c)^2[|\gamma_{1,2}|^4 + (1+|\gamma_{1,2}|^2)^2]}}\,, \tag{33}$$

where $\gamma_{1,2} \equiv \gamma_{1,2}(0)$, and $N \equiv \eta(T_c/T)\int_0^T \mathrm{d}t\,\langle|E_m(t)|^2\rangle$, for $m = 1, 2$, is the mean photoelectron number per temporal mode (or equivalently per coherence time) of the fields incident on the detectors. The terms in the denominator have intuitive interpretations. The first term, which is independent of $N$, is due to the shot noise of the two detectors. The third term, with the $N^2$ dependence, is excess noise resulting from the statistical fluctuations of the incident power on the detectors. This term is sometimes referred to as relative intensity noise. The middle term, with the $N$ dependence, is a result of the beating between the intensity fluctuations and shot noise. In the shot-noise limited regime $N \ll 1$ holds, i.e., the mean number of photoelectrons *per mode* is very small, and the SNR can be approximated as

$$\mathrm{SNR} = \frac{\sqrt{TT_B}}{T_c}|\gamma_{1,2}|^2 N. \tag{34}$$

Therefore the SNR has a quadratic dependence on the incident photon flux per mode. In the opposite regime with many photoelectrons per mode, thus $N \gg 1$, the SNR saturates to its maximum value

$$\mathrm{SNR} = \sqrt{\frac{T}{T_B}}\frac{|\gamma_{1,2}|^2}{\sqrt{|\gamma_{1,2}|^4 + (1+|\gamma_{1,2}|^2)^2}}\,. \tag{35}$$

For direct intensity measurements, we assume that a simple photon bucket operation is performed over $T$-seconds of integration,

$$D = \int_0^T \mathrm{d}t\, i(t), \tag{36}$$

where the statistics in Eqs. (29) and (30) are still true, but we assume that $\int \mathrm{d}t\, h_B(t) = 1$, such that the DC component is no longer filtered out. Again, defining

$$\mathrm{SNR} \equiv \frac{\langle D\rangle}{\sqrt{\langle (D - \langle D\rangle)^2\rangle}}\,, \tag{37}$$

it is straightforward to derive the SNR as

$$\mathrm{SNR} = \sqrt{\frac{T}{T_c}\frac{N}{1+N}}\,, \tag{38}$$

where all parameters are as defined before. Thus, when $N \ll 1$, the system is shot-noise limited and we have

$$\mathrm{SNR} = \sqrt{N\frac{T}{T_c}}\,, \tag{39}$$

whereas when $N \gg 1$ excess noise dominates and the SNR saturates at

$$\mathrm{SNR} = \sqrt{\frac{T}{T_c}}\,. \tag{40}$$

To separate the SNR dependence on the integration time $T$, which is common to both the correlation and direct intensity measurements, it is convenient to normalize it to $\sqrt{T/T_c}$. Fig. 11 shows thus normalized SNR of a direct intensity measurement (38) and the asymptotic approximations (34) and (35) of a correlation measurement SNRs, as functions of the mean photoelectron number per mode. As seen from this figure, the correlation measurement SNR can approach the direct-intensity measurement SNR for the sources with high spectral brightness, $N \approx 1$. The correlation-based measurements typically have worse SNR than direct-intensity measurements when shot-noise limited due to the dependence on the square of the incident average photon number in correlation measurements rather than just the photon number in direct intensity measurements. However in the excess-noise limited regime, the correlation measurements' SNR improves due to the fact that such measurements can distinguish source fluctuations from those caused by an object better than the direct-intensity measurement. Note, however, these plots compare the SNRs when the photoelectrons per mode are equal in both methods. Whereas correlation-based measurements require that $T_B < T_c$, thereby limiting the total flux incident on the detector, the direct intensity measurement can integrate over a very wide optical bandwidth, without penalty. We have already discussed this aspect of correlation imaging technique in Section II considering the example of Solar spectrum.

Thus, in general, the SNR in the correlation measurement is worse than in the direct intensity measurements. Nonetheless, in order to have a realistic assessment of the added value of correlation-based measurements for imaging

space objects, one must take into account stray light, detector aging, natural variation of source brightness and other practical effects that are usually omitted in the SNR analyses published to date. The detectors' dark noise may be particularly important in cases when the incident photons flux is low. On the other hand, the correlation technique may be particularly beneficial for narrow-band imaging, e.g. imaging using a specific bright or dark spectral line. A narrow spectral feature will lead to the higher spectral brightness and give the correlation imaging advantage according to Fig. 11.

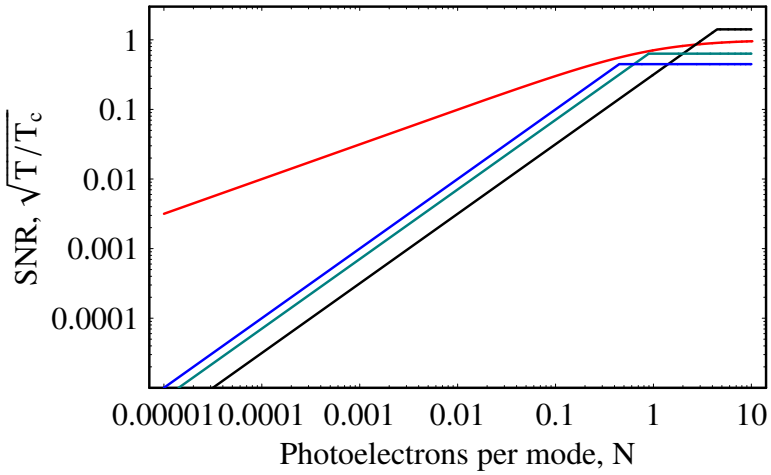


FIG. 11: The normalized intensity SNR (red) and correlation measurement SNR for $T_B/T_c = 0.1$ (the lowest), 0.5 and 1.

## VIII. CONCLUSIONS AND PHASE II OUTLOOK

During our Phase I NIAC research effort we have investigated the possibility of performing intensity correlation "ghost imaging" of dark amplitude and phase objects in space illuminated by thermal light sources (stars). Our approach hinges on replacing the beam splitter, indispensable for thermal light ghost imaging but infeasible for space imaging, with the object itself. The absorptive and refractive properties of the object are predicted to imprint themselves on the intensity correlation properties of the transmitted and scattered light and could be extracted from the correlation measurements. To test this concept we limited our discussion to fully analytical model relying on a two-dimensional source and an object with Gaussian distribution of luminosity, absorption or phase delay (the latter representing a thin lens) in paraxial approximation. We demonstrated the variation of the far-field speckle size due to the presence of the object. We have shown that the speckle size variation is a non-trivial function of the object's properties and position. In some cases it allows us to distinguish different phase and amplitude objects even when they produce very similar shadows and can hardly be distinguished by a direct intensity measurement. Thus the correlation measurement provides a complimentary information to a direct observation.

This understanding has encouraged us to apply our analytical model to a realistic space object imaging scenario, such as the Kepler mission. Our prediction for the flux variation very close to the actual observation. It also predicted a similar (about $10^{-4}$) fractional variation of the speckle size. We have carried out a preliminary SNR analysis for a correlation measurement, comparing it to a direct flux measurement. The analysis has shown that, for parameters typical of the Kepler mission, the correlation measurement SNR would be significantly worse than the intensity measurement SNR. This analysis however does not include certain instrumental types of noise, that may be detrimental for the intensity measurement more than for the correlation measurement and could potentially balance or even reverse the SNRs inequality. These are the dark noise and variation of detector's responsivity (quantum efficiency) due to environmental fluctuations and aging. The ambient background light is another important factor that needs to be considered. We plan to include these factors in the advanced noise model which will be developed in the follow-on research.

Regardless of the technical noises, the correlation measurement SNR improves relative to the intensity measurement SNR when the spectral brightness of the signal increases. Thus the correlation measurement may be especially advantageous in narrow-band imaging, e.g. imaging based on a selected spectral line. As a final note, comparison of the SNRs of two types of measurement is the decisive criterion when the measurements provide the same type of information. As we have seen, the correlation measurement can provide information additional to the intensity

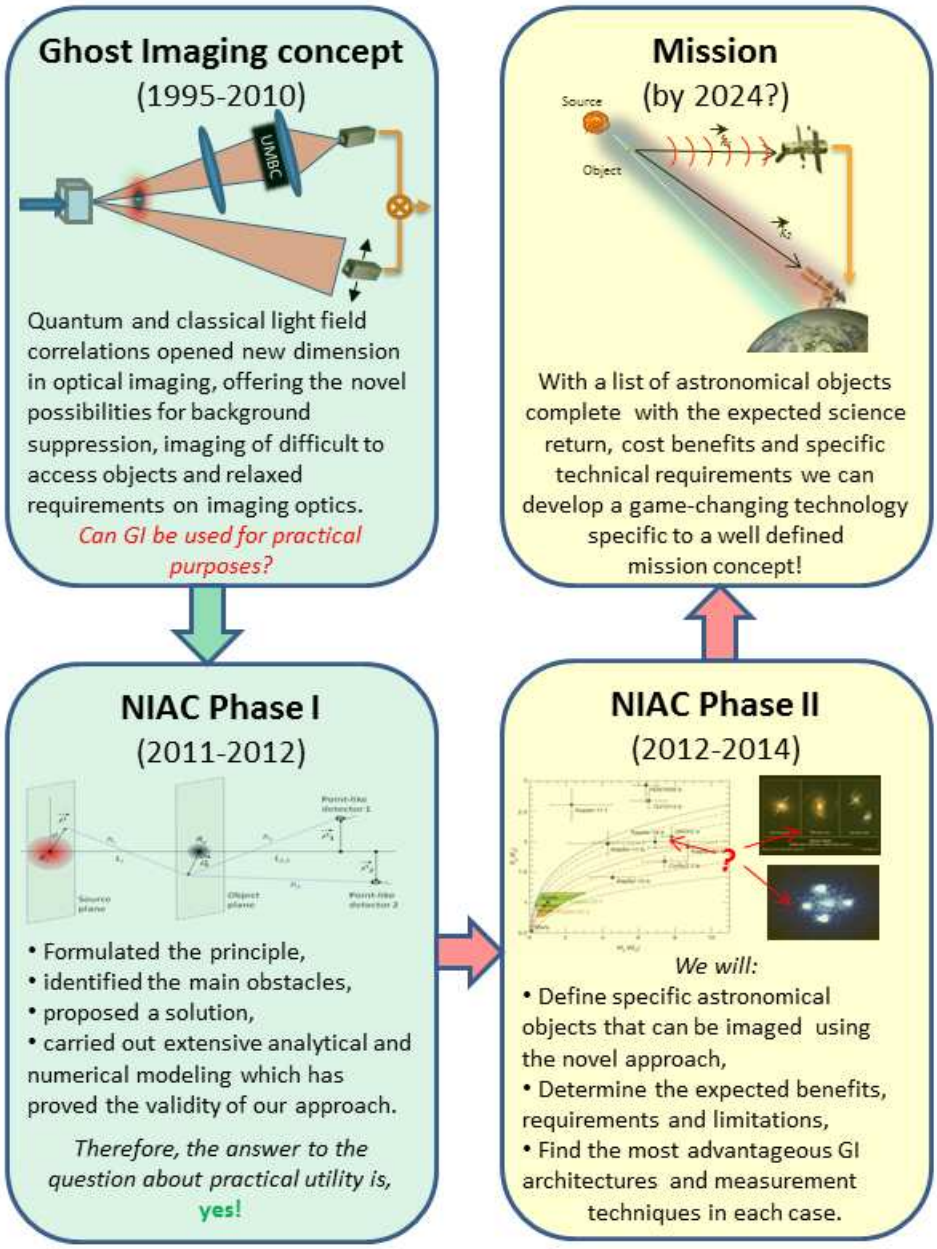


FIG. 12: Our vision of the relations between the underlying Ghost Imaging concept, the results of Phase I research, the Phase II plans, and the future NASA missions.

measurement. Moreover, for predominantly phase space object (such as e.g. a gravitational lenses or dilute gas clouds) producing little or no tell-tale shadows but affecting the optical coherence, correlation ghost imaging may be the preferred option.

Based on these results we conclude that further research in this direction will be advantageous. We have submitted the Phase II proposal, which has been awarded. The programmatic relations between the Phase I and Phase II NAIC research and potential future missions is shown in Fig. 12. According to this diagram, the main focus of the Phase

II research will be made on identifying specific astronomic objects whose exploration could benefit the most from application of the correlation imaging techniques, as well as determining the imaging techniques that would be the most efficient. By the latter we mean, in particular, the type of observable to be used for the imaging. The most typical observation in the ghost imaging is done in terms of the Glauber second-order correlation function (5). Most of the analysis that we carried out so far was done for this type of observable, which makes our approach a close relative of the intensity interferometer. However in contrast with the conventional intensity interferometry, this is not the only option. It has been shown [25] that higher contrast images can be obtained if Eq.(5) is generalized for higher powers of intensities. The optimization of these powers has also been discussed [26]. Applying this technique to our imaging architecture may allow us to further increase the imaging contrast and background suppression. Another novel detection technique [19, 21] relies on measuring a variance of the difference of two detectors signal, rather than on photo counts coincidences (i.e., a product). The photocurrent measurements are preferred in cases when the light signals are not too weak, as they give access to high quantum efficiency detectors and higher detection bandwidths.

These alternative detection techniques may offer interesting trade-offs in terms of the resolution, SNR and instrument requirements, and therefore should be studied. The required analytical and numerical computations are very similar to those we performed for Glauber correlation functions. Indeed, the part of the analysis that describes the optical field propagation from the source to the detectors, and also includes the object's model, will be the same. This is the most extensive and complex part of the analysis. Therefore it appears logical to investigate the alternative detection techniques when the object modeling is fully understood and developed.

The technical task of the Phase II research that will support its main goal can be summarized into the following list:

1. Develop numerical models better approximating the real space objects: opaque disks, randomly scattering objects, phase objects mimicking gravitational lenses. Investigate simple 3D models and determine if they can be sufficiently accurately approximated by flat objects.

2. If in step 1 it is established that 2D modeling in some important cases cannot be adequate, develop analytical 3D models for simple objects and numeric models for more realistic objects.

3. Investigate the potential benefits of using other types of observables (higher-order correlation functions, intensity difference variance).

4. Carry out a lab demonstration of different imaging strategies.

5. Based on the results from steps 1 and 2, compile a list of astronomical objects that potentially could be observed by one of the types of ghost imaging.

6. Carry out the data rate, SNR, resolution (if applicable), contrast, observation baseline and other fundamental parameters estimates for the selected objects. Verify that application of our approach is indeed practical and beneficial.

7. Based on the results from step 5, compile a short list of astronomical objects of interest, complete with the fundamental observation requirements and constraints specific for each object.

Successful implementation of the Phase II will significantly upgrade the missions relying on conventional optical observation and detection techniques. While the maturity period of the proposed technology is estimated to be of the order of up to ten years, and the benefiting missions are not yet proposed, the contemporary missions that could benefit from this technology can be already pointed out. These include the aforementioned Kepler and similar planetary detection missions; Hubble space telescope one of whose objects of interest are gravitational lenses, as well as other space and ground-based telescopes included into SOFIA program; GALEX and other similar missions. We do not anticipate any conceptual change in the impacted missions' architecture. Instead, by adding a second observer and implementing a correlation measurement protocol in addition to the standard intensity (photon flux) measurement, we expect to significantly increase the science data return from these missions. The additional data will be complimentary to the intensity measurement data in that it may provide more information about the object's scattering, absorptive and refractive properties as well as the geometrical relations between the object and source sizes and object-source, object-detectors distances. The correlation data may be received in the spatially-resolved (for the case of optical imaging) or unresolved (for the case of optical detection) format. Therefore we plan to significantly

enhance the future missions scientific return with only an incremental increase of their cost.

## IX. REFERENCES


[1] J.J. Lissauer et al., Nature **470**, 53-58 (2011).
[2] F. Fressin et al., Nature **482**, 195-198 (2011).
[3] Hanbury R. Brown and R.Q. Twiss, Proc. of the Royal Society of London, A, **242** 300-324 (1957); Hanbury R. Brown and R.Q. Twiss, Proc. of the Royal Society of London, A, **243** 291-319 (1958).
[4] I. Klein, M. Guelman, and S. G. Lipson, Appl. Opt. 46, 4237-47 (2007).
[5] L. A. Lugiato, A. Gatti and E. Brambilla, J. Opt. B: Quantum Semiclass. Opt. **4**, S176S183 (2002).
[6] Agedi N. Boto, Pieter Kok, Daniel S. Abrams, Samuel L. Braunstein, Colin P. Williams, and Jonathan P. Dowling, Phys. Rev. Lett., **85**, 2733-2736 (2000).
[7] Milena DAngelo, Maria V. Chekhova, and Yanhua Shih, Phys. Rev. Lett., **87**, 013602 (2001).
[8] K.W.C. Chan, M.N. OSullivan, and R.W. Boyd, Phys. Rev. A, **79**, 033808 (2009).
[9] D. Yu. Korystov, S. P. Kulik, and A. N. Penin, JETP Letters, **73**, No. 5, 214218, (2001).
[10] R. Meyers, K.S. Deacon and Y. Shih, Phys. Rev. A, **77**, 041801(R) (2008).
[11] T.B. Pittman, Y.H. Shih, D.V. Strekalov, and A.V. Sergienko, Phys. Rev. A, **52**, R3429 (1995);
[12] D.V. Strekalov, A.V. Sergienko, D.N. Klyshko, Y.H.Shih, Phys. Rev. Lett., **74**, 3600 (1995).
[13] A. Gatti, E. Brambilla, M. Bache, and L. A. Lugiato, Phys. Rev. A, **70**, 013802 (2004); A. Gatti, E. Brambilla, M. Bache, and L. A. Lugiato, Phys. Rev. Lett, **93**, 93602 (2004);
[14] Alejandra Valencia, Giuliano Scarcelli, Milena DAngelo, and Yanhua Shih, Phys. Rev. Lett., **94**, 063601 (2005).
[15] L.-G. Wang, S.Qamar,S.-Y. Zhu, and M.S. Zubairy, Phys. Rev. A, **79**, 033835 (2009).
[16] J. H. Shapiro, Phys. Rev. A, **78**, 061802(R),(2008).
[17] B.I. Erkmen, and J.H. Shapiro, Advances in Optics and Photonics **2**, 405450 (2010).
[18] T. Iskhakov, A. Allevi, D. A. Kalashnikov, V.G. Sala, M. Takeuchi, M. Bondani, and M.V. Chekhova, Eur. Phys. J. Special Topics **199**, 127-138, (2011).
[19] G.Brida, M.V. Chekhova, G.A. Fornaro, M. Genovese, L.Lopaeva, I. RuoBerchera, Phys Rev. A **83**, 063807 (2011).
[20] R. J. Glauber, Phys. Rev. **130**, 2529-2539, (1963).
[21] E.Lopaeva and M. Chekhova, JETP Lett. **91**, 447 (2010).
[22] `http://www.nrel.gov/solar_radiation/`
[23] J.G. Cramer, Phys. Rev. D, **22**, 362-376 (1980); J.G. Cramer, Rev. of Mod. Phys., **58**, 647 (1986); D.N. Klyshko, Phys. Lett. A, **128**, 133-137, (1988).
[24] H. Gamo, JOSA **56**, 441-451 (1966).
[25] Xi-Hao Chen, Ivan N. Agafonov, Kai-Hong Luo, Qian Liu, Rui Xian, Maria V. Chekhova, and Ling-An Wu, Opt. Lett. **35**, 1166 (2010).
[26] K. W. C. Chan, M. N. O'Sullivan, and R. W. Boyd, Opt. Express **18**, 5562 (2010).